12th INTERNATIONAL SCIENTIFIC CONFERENCE ON DEFENSIVE TECHNOLOGIES
OTEH 2026
Serbia, Tara, 21 - 24 October 2026

MAGNETOIMPEDANCE EFFECT OF $Fe_{72}Al_5Ga_2P_{11}C_6B_4$ AMORPHOUS RIBBON

RADOSLAV SURLA
Military Technical Institute, Belgrade, Serbia, ekorade@gmail.com

JOVANA MANDIĆ
Military Technical Institute, Belgrade, Serbia, jmandic96@gmail.com

JELENA ORELJ
Faculty of Technical Sciences, University of Kragujevac, Serbia, jelena.orelj@ftn.kg.ac.rs

NEBOJŠA MITROVIĆ
Faculty of Technical Sciences, University of Kragujevac, Serbia, nebojsa.mitrovic@ftn.kg.ac.rs

PAVEL CRNOMARKOVIĆ
Military Technical Institute, Belgrade, crnomarkovic.pavel@gmail.com

Abstract: *The paper presents the results of an experimental investigation of the magnetoimpedance (MI) response of an $Fe_{72}Al_5Ga_2P_{11}C_6B_4$ amorphous ribbon, prepared by the melt-spinning rapid quenching technique on a rotating copper wheel. Characterization revealed that the internal configuration and the profile of the MI curves exhibit a strong frequency dependence, reaching a maximum MI ratio value of 31.3% at an operating frequency of 36.11 MHz without an external magnetic field. With an increase in the magnetic field intensity, a continuous decrease in the MI ratio values is observed. At frequencies above 75 MHz, slight distortions in the profile of the experimental curves are noticed at a field strength of approximately 8 kA/m, which hints at the presence of an internal magnetic anisotropy field. Considering the completely amorphous structure of the sample in the as-cast state, this aspect cannot be analyzed in more detail at this stage; however, its clear expression and dominant influence on the soft magnetic properties are expected after the thermo-activated transformation of the amorphous matrix into a nanocrystalline state via controlled isothermal annealing.*

Keywords: *Magnetoimpedance effect, Amorphous alloys, Melt-spinning, Magnetic anisotropy.*

1. INTRODUCTION

The phenomenon of magnetoimpedance (MI) represents a specific electromagnetic response observed in a narrow group of soft magnetic alloys with an amorphous or nanocrystalline structure. This effect is manifested through an intensive variation in the complex impedance of a ferromagnetic sample under the influence of an external direct current (DC) magnetic field. Since its discovery at the end of the last century, this phenomenon has become a fundamental platform for the development of high-sensitivity magnetic field sensors used in automotive, military, and aerospace industries [1-8].

It has been experimentally proven that the impedance module of a ferromagnetic material decreases with an increase in the external field intensity, while simultaneously increasing with the frequency of the excitation current flowing through the sample. Quantification of this effect is most commonly performed by defining the MI ratio according to the following equation:

$$\Delta Z/Z(\%)=100\% \cdot (Z(H)-Z(H_{max}))/Z(H_{max}), \quad (1)$$

where $Z(H_{max})$ represents the reference impedance value measured at the maximum intensity of the applied external magnetic field. Depending on the internal magnetic configuration and processing technology, under zero-field conditions (H = 0), the influence of remanent magnetization may come into play, the disappearance of which with an increasing field causes a characteristic asymmetry in the MI diagrams for opposite directions of the applied field (for the -H and +H directions).

The frequency dependence of the magnetoimpedance is directly induced by the skin effect, which is described by the equivalent penetration depth of the current through the conductor. This value increases due to the drop in the total magnetic permeability in a strong magnetic field, while it decreases with increasing frequency. The action of a high-frequency alternating current induces strong eddy currents in the sample, causing the displacement of charge carriers and the concentration of electrical energy towards the peripheral regions of the conductor. The penetration depth is defined by the following relation:

$$\delta_m=(\rho/(\pi \cdot \mu \cdot f))^{0.5}, \quad (2)$$

where σ is the electrical conductivity, μ is the magnetic permeability, and f is the frequency of the alternating current. In addition to pure electromagnetic parameters, the MI response is crucially influenced by the domain structure of the magnetic material, which is a direct function of the internal structural arrangement and the applied sample geometry. Therefore, the maximum values of the MI ratio

Corresponding author: R.Surla;
E-mail: ekorade@gmail.com

DOI: 10.5937/OTEH26137S

represent a compromise between the frequency and the strength of the magnetic field, which is precisely defined by experimental measurements.

2. EXPERIMENTAL PROCEDURE

The subject of experimental investigations in this study is a multi-component alloy with the composition $Fe_{72}Al_5Ga_2P_{11}C_6B_4$. Samples were synthesized in the form of thin ribbons (geometric dimensions: width about 2 mm, thickness about 40 μm) by applying the technology of ultra-rapid quenching of the liquid alloy melt on a rotating copper wheel (melt-spinning method) in a protected atmosphere.

The characterization of the magnetoimpedance (MI) effect was performed in a homogeneous external magnetic field with a maximum intensity up to 15 kA/m, which was generated using a custom-designed and controlled system with two pairs of Helmholtz coils providing field homogeneity above 99% [5, 9]. The measurement of the complex impedance of the investigated ribbon samples was realized in a wide frequency range using a vector network analyzer (instrument: Vector Network Analyzer Agilent 8753ES).

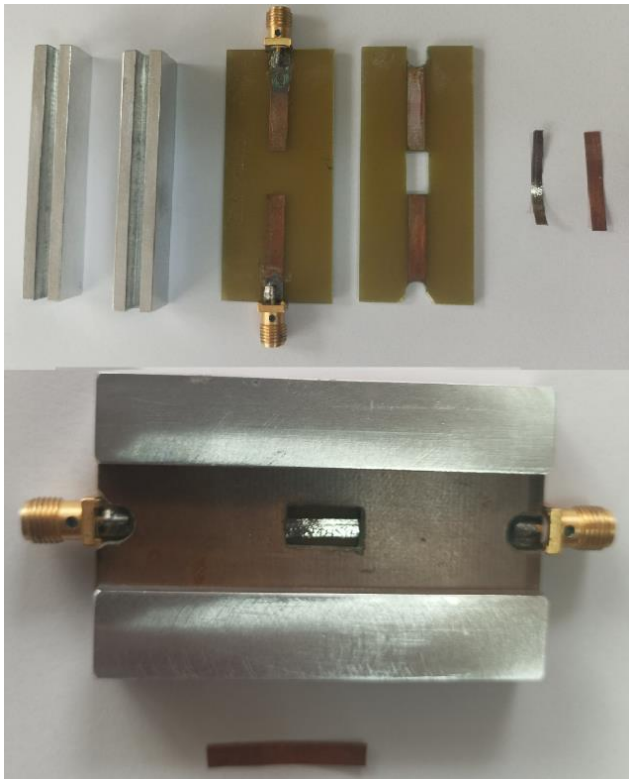


Figure 1. Sample holder configuration: (top) components of the microstrip holder, (bottom) amorphous ribbon sample positioned within the holder, showing the short-circuit element used for network analyzer calibration.

The sample holder was specifically designed in the form of a microstrip to accommodate the specific geometry of the investigated ribbon (Figure 1). The ends of the electrical contacts were placed at a fixed distance of 1 cm, while the total length of the measured ribbon was at least 2 cm to eliminate the influence of contact resistances at the connection points. The measurement is realized by connecting to a single port of the instrument, which automatically converts the reflection S_{11} parameters into the impedance of a 1 cm long sample. The systematic error introduced by the cables and the holder itself was eliminated by precise calibration of the measurement setup using a copper short-circuit jumper of similar dimensions.

The structural properties of the obtained ribbons in the initial state were investigated by X-ray diffraction (XRD) on a Rigaku SmartLab apparatus using a Cu Kα radiation source. The identification of the amorphous nature of the material was performed based on the shape and geometry of the diffraction lines recorded at room temperature. The surface morphology and topography of the free side of the amorphous ribbon were analyzed using scanning electron microscopy (SEM JEOL JSM-6610-LV), while the chemical homogeneity and quantitative composition of the constituent elements of the alloy were verified by energy-dispersive X-ray spectroscopy (EDS).

3. RESULTS AND DISCUSSION

3.1 XRD Analysis

X-ray structural analysis (XRD) confirmed the amorphous character of the synthesized ribbon in the initial as-cast state. In the obtained diffractogram (Figure 2), only a characteristic broad diffraction maximum (the so-called amorphous halo) is observed in the 2θ angle range between 40° and 50°. The complete absence of any sharp and intense Bragg reflections clearly indicates the absence of long-range crystalline order within the investigated material. This appearance of the diffraction profile unequivocally confirms that the applied ultra-rapid melt quenching technology successfully suppressed premature crystallization processes and effectively froze the structural disorder in the sample.

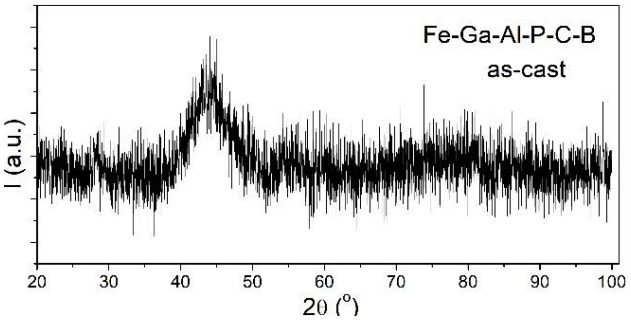


Figure 2. XRD pattern of the $Fe_{72}Al_5Ga_2P_{11}C_6B_4$ amorphous ribbon in the as-cast state.

3.2 SEM and EDS Analysis

Scanning electron microscopy (SEM) was applied for direct investigation of the surface morphology of the free (shiny) side of the cast ribbon. The micrograph shown in Figure 3 demonstrates high structural homogeneity and surface smoothness, without the presence of microporosity, cracks, or early crystal nuclei that could degrade the magnetic softness of the ribbons.

Concurrently, EDS analysis (Figure 4) was used for detailed chemical characterization of the sample. The results of quantification in atomic and weight fractions,

summarized in Table 1, confirm that the experimentally determined composition completely corresponds to the nominal stoichiometry of the $Fe_{72}Al_5Ga_2P_{11}C_6B_4$ alloy, testifying to the high chemical uniformity of the material along the entire ribbon sample.

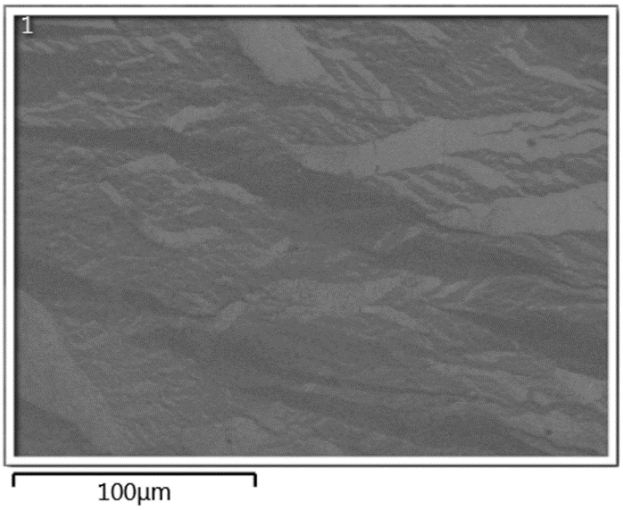


Figure 3. SEM micrograph of the free (shiny) side of the $Fe_{72}Al_5Ga_2P_{11}C_6B_4$ amorphous ribbon.

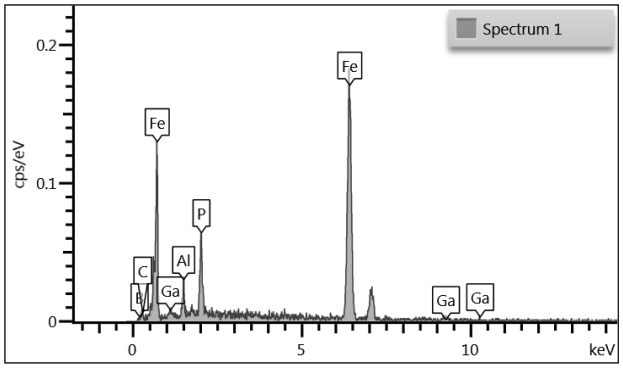


Figure 4. SEM-EDS spectrum and elemental analysis of the as-cast $Fe_{72}Al_5Ga_2P_{11}C_6B_4$ amorphous ribbon.

Table 1. Quantitative elemental composition (weight and atomic percentages) of the investigated $Fe_{72}Al_5Ga_2P_{11}C_6B_4$ amorphous ribbon.

Element	Wt%	Atomic %
B	3.00	11.68
C	3.25	11.37
Al	3.49	5.44
P	7.11	9.64
Fe	78.43	59.03
Ga	4.71	2.84
Total:	100.00	100.00

3.3 Magnetoimpedance Measurements

The diagram in Figure 5 shows the MI ratio as a function of the excitation current frequency for different values of the external magnetic field. Experimental characterization established that the MI effect is highly pronounced in the frequency interval from 17 MHz to 40 MHz. The MI ratio reaches its maximum value at a frequency of 36.11 MHz under zero external field conditions (H = 0 A/m) and amounts to 31.3%.

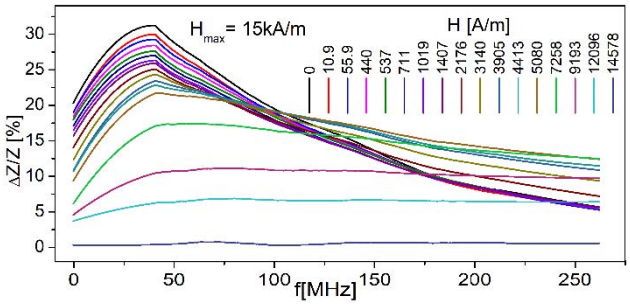


Figure 5. Frequency dependence of the MI ratio for different external magnetic field strengths up to H_{max} = 15 kA/m.

Analysis of the diagrams in Figures 5 to 8 reveals a constant, monotonic decreasing trend of the MI ratio with an increase in the magnetic field intensity acting longitudinally on the measured sample. This decrease in impedance is a consequence of the rotation of the magnetization vector in the direction of the external magnetic field. Also, the profile of the MI curves shows constant growth with increasing frequency up to 36.11 MHz (Figure 6), while with a further increase in frequency above this value, the curves are in a noticeable decline (Figure 8).

At frequencies higher than 75 MHz, specific deformations and distortions of the experimental curve profiles are observed at an external magnetic field strength of around 8 kA/m. Considering that the investigated alloy is completely amorphous in the initial state, this phenomenon cannot be analyzed or quantified in detail at this stage of the research; instead, the mentioned distortions serve as an early indication that only hints at the presence of an internal magnetic anisotropy field. This anisotropy is currently overshadowed by internal stresses generated during the rapid cooling of the liquid alloy melt [10 - 12].

Further insight into the frequency range from 18 to 36 MHz shows that the curves are almost completely overlapped (Figure 7). Therefore, it is expected that a controlled thermo-activated treatment (annealing) will lead to structural relaxation and transformation of the amorphous matrix into a two-phase nanocrystalline structure (with a dominant α-Fe(Si) phase), which will enable a clear expression of the magnetic anisotropy field and a drastic improvement in the MI performance, which will be the subject of our future work.

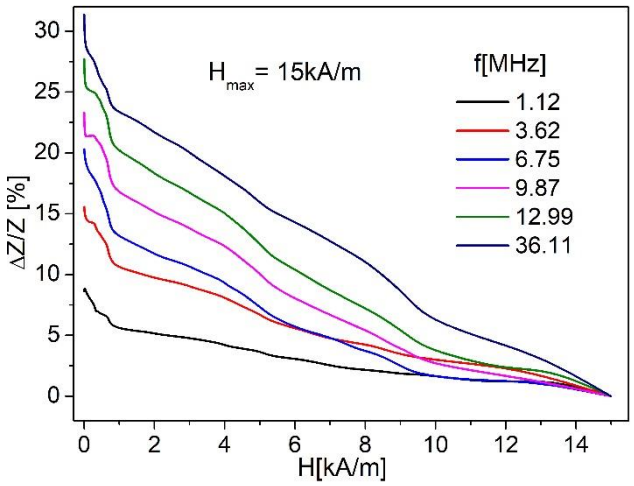


Figure 6. Magnetic field dependence of the MI ratio profiles at low excitation current frequencies ranging from 1.12 MHz to 36.11 MHz.

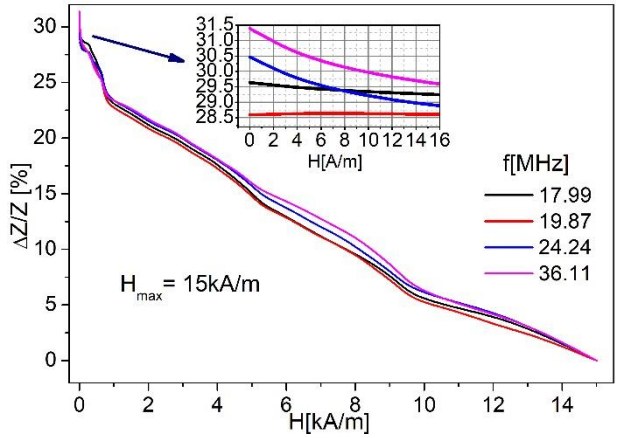


Figure 7. Superposition and convergence of the MI ratio curves in the optimal frequency range from 17.99 MHz to 36.11 MHz.

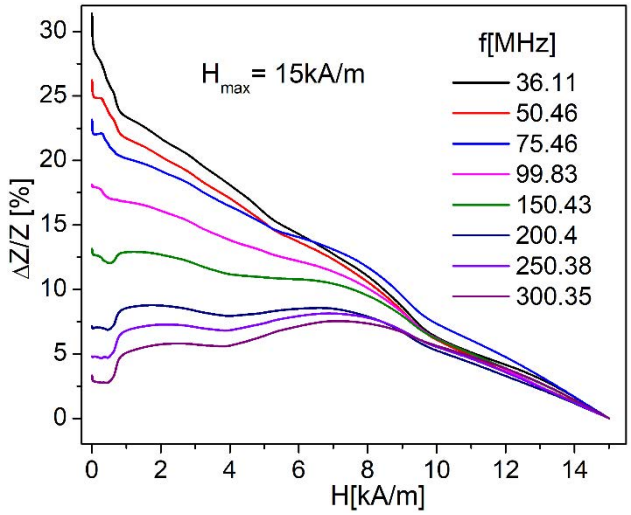
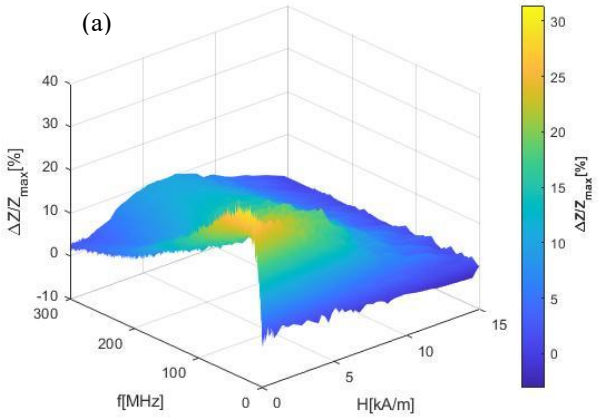
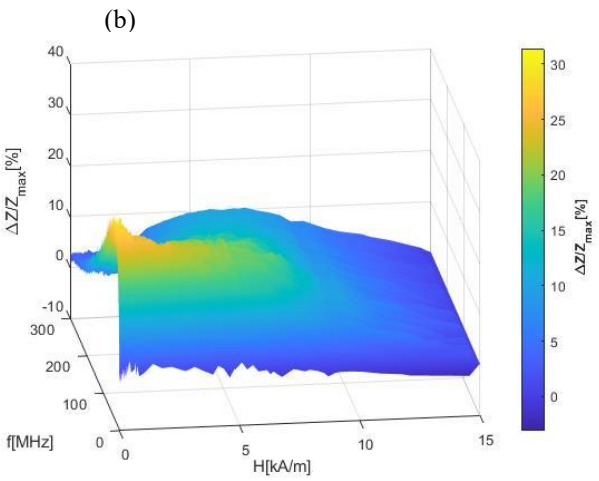


Figure 8. Magnetic field dependence of the MI ratio profiles at high frequencies from 36.11 MHz to 300.35 MHz, showing profile distortions near 8 kA/m that hint at the internal magnetic anisotropy.

In order to comprehensively evaluate the simultaneous influence of the excitation current frequency and the external magnetic field strength on the magnetoimpedance properties of the investigated alloy, three-dimensional dependence diagrams along with a corresponding two-dimensional projection map were constructed, as presented in Figure 9. On the three-dimensional surface plots (Figures 9a and 9b), the spatial profile of the MI response is clearly and explicitly observed across the entire measured frequency range up to 300 MHz. This representation allows an unequivocal insight into the curve evolution, where a dominant peak of the MI ratio stands out at 36.11 MHz under low external field conditions, followed by a symmetrical drop in impedance with increasing field strength due to the magnetic saturation of the sample. On the other hand, the 2D projection color map from the top view (Figure 9c) provides a precise topographic overview of the impedance contours, where the optimal frequency zone for the stabilization of the effect is distinctly demarcated colorimetrically. These visualizations confirm the high linearity and sensitivity of the MI response in the characteristic domain, establishing a crucial experimental foundation for the precise engineering of future magnetic sensors based on this amorphous ribbon.





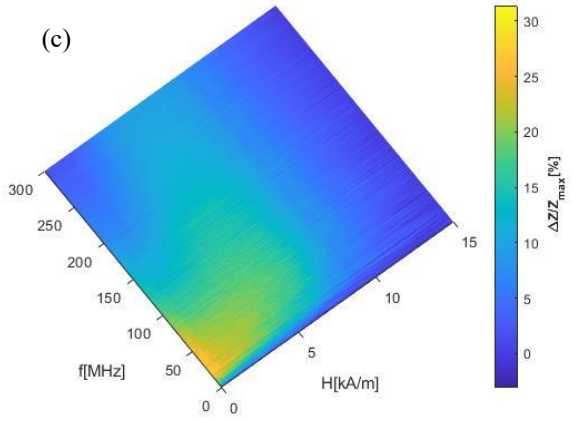


Figure 9. Magnetoimpedance (MI) ratio profiles as a multi-variable function of the excitation current frequency ,f and external magnetic field strength**: (a)** 3D surface plot from the front view emphasizing low-frequency peaks, **(b)** 3D surface plot from the rear view illustrating the high-frequency drop and profile distortions, and **(c)** 2D projection color map (top view) highlighting the optimal operational frequency window and convergence zones.

5. CONCLUSION

In this work, the magnetoimpedance response of an amorphous ribbon of a multi-component $Fe_{72}Al_5Ga_2P_{11}C_6B_4$ alloy obtained by the melt-spinning method was successfully evaluated. It was experimentally confirmed that the investigated material achieves its optimal MI profile at a characteristic frequency of 36.11 MHz, where the value of the MI ratio is 31.3% in the absence of a field. The shape and trend of the obtained curves show a high sensitivity to changes in the frequency of the excitation signal.

At high frequencies above 75 MHz and at a field strength of 8 kA/m, specific curvatures of the experimental curves were observed, representing an early indication and a hint of the existence of a magnetic anisotropy field. Since this phenomenon is overshadowed by structural disorder and residual casting stresses in the initial state, a complete analytical picture of the anisotropy field, as well as the projected increase in magnetic softness and sensitivity of the sensor element, are planned in the next phase through controlled isothermal annealing and the generation of a stable nanocrystalline matrix.

Acknowledgement

This work was supported by the Ministry of science, technological development and innovations (Serbia), Contract No. 451-03-34/2026-03/200325.

References

[1] Panina, L.V., Mohri, K.: *Magneto-impedance Effect in Amorphous Wires*, Applied Physics Letters, 65(9), (1994), 1189 – 1191.

[2] Kraus, L.: *Theory of Giant Magneto-impedance in the Planar Conductor with Uniaxial Magnetic Anisotropy*, Journal of Magnetism and Magnetic Materials, 195(3), (1999), 764 – 778.

[3] Surla, R., Mitrović, N., Đukić, S., Ibrahimović, V.: *Amorphous $Fe_{72}Cu_1V_4Si_{15}B_8$ Ribbon as Magneto-Impedance Sensing Element*, Serbian Journal of Electrical Engineering, 13(3), (2016), 381-394.

[4] Surla, R., M., Vasić, Mitrović, N., Radović, Lj., Minić, D.: *Magnetic properties of* $Fe_{72}Cu_1V_4Si_{15}B_8$ *alloy with a composite amorphous/ nanocrystalline structure,* Journal of Magnetism and Magnetic Materials, 564 (2022) 170141

[5] SURLA, R.: Doktorska disertacija: *Uticaj odgrevanja na strukturne transformacije i magnetna svojstva legure $Fe_{72}Cu_1V_4Si_{15}B_8$,* FTN Čačak, Univerzitet u Kragujevcu, 2021.

[6] Vasić M., Surla R., Mitrović N., Minić Dragica., Mitrović N., Maričić A., Minić Dušan: *Thermally induced microstructural transformations of $Fe_{72}Cu_1V_4Si_{15}B_8$ alloy*, Metal. Mater. Trans. A 48 (2017) 4393–4402.

[7] Surla, R., M., Vasić, Mitrović, N., Minić, D.: *Synthesis and characterization of $Fe_{72}Cu_1V_4Si_{15}B_8$ metallic glass ribbons prepared by melt spinning casting*, 9th International Scientific Conference on Defensive Technologies, Belgrade, 8-9, October 2020.

[8] Surla, R., Mitrović, N., Orelj, J., Crnomarković, P.: *Magnetoimpedance effect of nanocrystalline FeNiSiB and FeCuVSiB ribbons*, 11th International Scientific Conference on Defensive Technologies, Belgrade, 9-11, October 2024.

[9] Surla, R., Mitrović, N., Crnomarković, P.: *Designing the controlled generator of a homogeneous magnetic field*, *10th International Scientific Conference on Defensive Technologies*, Belgrade, 13-14, October 2022, ID 116, ISBN 978-86-81123-85-0.

[10] Herzer, G.: *Grain structure and magnetism of nanocrystalline ferromagnets*, IEEE Transactions on Magnetics, 25 (1989) 3327-3329.

[11] Kulik, T.: *Nanocrystallization of metallic glasses*, Journal of Non-crystalline Solids, 287 (2001) 145-161.

[12] Herzer, G.: *Anisotropies in soft magnetic nanocrystalline alloys*, Journal of Magnetism and Magnetic Materials, 294 (2005) 99-106.